Eur. J. Biochem. **267**, 4054–4062 (2000) © FEBS 2000

Mutational analysis of arginine 177 in the nucleotide binding site of β-actin

Herwig Schüler[1], Maria Nyåkern[1], Clarence E. Schutt[2], Uno Lindberg[1] and Roger Karlsson[1]

[1]*Department of Cell Biology, The Wenner-Gren Institute, Stockholm University, Sweden;* [2]*The Henry Hoyt Laboratory, Department of Chemistry, Princeton University, NJ, USA*

Actin ADP-ribosylated at arginine 177 is unable to hydrolyze ATP, and the R177 side chain is in a position similar to that of the catalytically essential lysine 71 in heat shock cognate protein Hsc70, another member of the actin-fold family of proteins. Therefore, actin residue R177 has been implicated in the mechanism of ATP hydrolysis. This paper compares wild-type β-actin with a mutant in which R177 has been replaced by aspartic acid. The mutant β-actin was expressed in *Saccharomyces cerevisiae* and purified by DNase I-affinity chromatography. The mutant protein exhibited a reduced thermal stability and an increased nucleotide exchange rate, suggesting a weakened interdomain connection. The ATPase activity of G-actin and the ATPase activity expressed during polymerization were unaffected by the R177D replacement, showing that this residue is not involved in catalysis. In the presence of polymerizing salts, ATP hydrolysis by both wild-type Mg-β-actin and the mutant protein preceded filament formation. With the mutant actin, the initial rate of ATP hydrolysis was as high as with wild-type actin, but polymer formation was slower, reached lower steady-state levels, and the polymers formed exhibited much lower viscosity. The critical concentration of polymerization (A_{cc}) of the mutant actin was increased 10-fold as compared to wild-type actin. Filaments formed from the R177D mutant β-actin bound phalloidin.

Keywords: ATPase activity; polymerization; nonmuscle actin; DNase I; phalloidin.

Incorporation of actin monomers (G-actin) into filaments (F actin) *in vitro* is accompanied by hydrolysis of ATP and subsequent release of inorganic phosphate. The result of this process is a difference in the properties of the two filament ends, which at steady state of polymerization is expressed as a slow polymerization/depolymerization and continued slow hydrolysis of ATP (treadmilling). *In vivo*, the turnover of actin filaments is much more dynamic involving a large number of proteins in the formation of cell surface projections and execution of a variety of motile activities. Hydrolysis of ATP on actin is thought to play a crucial role in the control of the turnover of actin filaments, but the mechanism and exact role(s) of the actin ATPase activity remains to be elucidated.

Actin shares its domain structure and nucleotide binding fold with the 70-kDa heat shock cognate proteins (Hsc70) and the sugar kinases [1]. The molecule consists of two major domains, each of which is divided into two subdomains [2–5]. The nucleotide:cation complex is bound at the bottom of the cleft between the major domains. Recently, a lysine (K71) was found to be the essential catalytic residue for nucleotide hydrolysis by the 44-kDa N-terminal ATPase domain of Hsc70 [6]. While the corresponding position in the actin sequence is occupied by a glycine, the guanidinium group of R177 in actin could be positioned similarly to the ε-amino group of K71 in Hsc70. The R177 side chain extends from the core of subdomain 3 towards the terminal phosphate group of the bound ATP (Fig. 1). Actin is ADP-ribosylated at R177 by various bacterial toxins (reviewed in [7]). This modification abolishes the ATPase activity of G-actin and inhibits actin polymerization [8,9]. For these reasons, R177 has been considered as a possible participant in ATP hydrolysis by actin.

Introducing the mutation R177A [10] or the double mutation R177A, D179A in yeast actin [11] caused a temperature-sensitive phenotype, and the absence of rhodamine-phalloidin staining of actin cables in the mutated yeast cells led to the conclusion that these residues are involved in phalloidin binding.

This paper describes the biochemical properties of isolated β-actin carrying the mutation R177D. The results demonstrate that arginine 177 can be changed to an aspartic acid residue without loss of ATPase activity. The formation of filaments from the mutated actin, however, was seriously disturbed leading to a greatly increased critical concentration of polymerization. Despite a reduced interdomain connectivity, the R177D mutant actin still bound DNase I, and filaments formed from the mutant β-actin bound phalloidin and fluorescein isothiocyanate (FITC)-phalloidin.

Correspondence to R. Karlsson, Department of Cell Biology, The Wenner-Gren Institute, Stockholm University, S-106 91 Stockholm, Sweden. Fax: + 46 8 159837, Tel.: + 46 8 164104, E-mail: Roger.Karlsson@cellbio.su.se

Abbreviations: A_{cc}, critical concentration for actin polymerization; FITC, fluorescein isothiocyanate.

Enzyme: deoxyribonuclease I (DNase I; EC 3.1.21.1)

(Received 2 March 2000, accepted 2 May 2000)

MATERIALS AND METHODS

Chemicals

Bovine pancreatic DNase I (crystalline) was from Chemicon ICN (Costa Mesa, CA, USA). Hydroxyapatite (even lot number) was from Clarkson Chromatography Products (South Williamsport, PA, USA). Rhodamine-phalloidin, FITC-phalloidin, $1,N^6$-ethenoadenosine 5′-triphosphate (εATP)

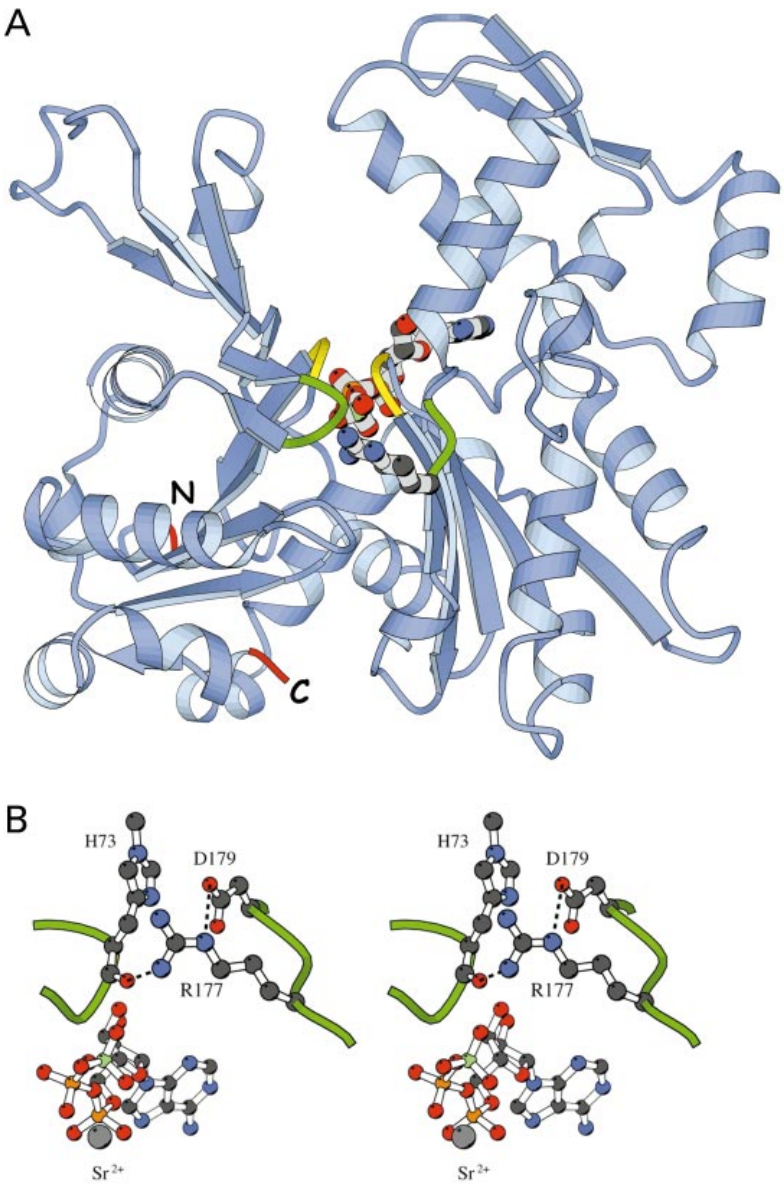

Fig. 1. Molecular representation of β-actin. (A) Overview of the molecule [4]. The bound nucleotide:cation complex and the side chain of R177 are shown. The phosphate binding loops in subdomains 1 and 3 are in yellow, and the two loops detailed in (B) are in green. The positions of the N- and C-termini in subdomain 1 are indicated. (B) Stereoview of actin-bound ATP and Sr^{2+}. The side chains of H73 in subdomain 2, and of R177 and D179 in subdomain 3 are shown. The molecular representations were made using MOLSCRIPT [48].

and *N*-(1-pyrene)iodoacetamide were from Molecular Probes (Eugene, OR, USA).

Mutagenesis and Protein Purification

Mutagenesis of the chicken β-actin gene, expression in *Saccharomyces cerevisiae* and isolation of the mutant β-actins followed previously published protocols [12,13]. Recombinant β-actin was kept on ice in G-buffer (5 mM Tris/HCl, pH 7.6, 0.5 mM ATP, 0.1 mM $CaCl_2$, 0.5 mM dithiothreitol, 0.006% NaN_3) and used within one week, or stored frozen as droplets in liquid N_2. Protein concentrations were determined spectrophotometrically, using an extinction coefficient of $E_{290} = 0.63\ mL{\cdot}mg^{-1}{\cdot}cm^{-1}$ for G-actin [14]. Exchange of the high-affinity Ca^{2+} for Mg^{2+} was achieved by incubating actin in G-buffer with 0.2 mM EGTA and 50 μM $MgCl_2$ for 15 min at room temperature [15]. Profilin and β/γ-actin were purified from bovine thymus [16]. All experiments were conducted at 25 °C.

DNase I–actin interaction

The affinity of the actin–DNase I interaction was determined from double-reciprocal plots of the dependence of DNase I inhibition on actin concentration using the DNase I inhibition assay [17].

Nucleotide exchange

G-actin (either Mg- or Ca-form) was freed from excess nucleotide by gel filtration in ATP-free G-buffer (with and without 0.2 mM EGTA and 50 μM $MgCl_2$, respectively), and the protein concentration was adjusted to 6 μM. After addition of 300 μM of εATP [18], the fluorescence increase at > 408 nm (excitation at 360 nm) was monitored using a Sigma ZWS II spectrofluorimeter (Biochem Wissenschaftliche Geräte GmbH, Puchheim, Germany). Off-rates for ATP were estimated by first-order curve fitting of the experimental data using ORIGIN (Micocal Software Inc., Northampton, MA, USA).

Thermal denaturation of actin

The DNase I inhibition assay [17] was used to assess the thermal stability of actin, as described in [19]. The T_m was defined as the temperature at which 50% of the initial DNase I inhibition activity (measured at 25 °C) was lost. The unfolding activation energies were estimated from Arrhenius plots of the apparent unfolding rate constants at different temperatures [19].

ATPase activity

Monomeric Ca-actin (16 μM) in G-buffer was incubated with 0.66 μM of [γ-^{32}P]ATP (3000 Ci·mmol^{-1}; Amersham Pharmacia), 50 μM Mg^{2+} and 0.2 mM EGTA for 10 min. The [γ-^{32}P]ATP-Mg-actin stock was diluted with Mg-G-buffer to the concentrations used. Actin ATPase activity was determined after addition of 1 mM $MgCl_2$ and 0.1 M KCl in the case of F-actin. At intervals, 2-μL aliquots of the reaction mixtures were applied onto TLC-plates (PEI-cellulose, Merck). After drying, thin layer chromatography was performed in 0.2 M ammoniumbicarbonate pH 8.0. Inorganic $^{32}P_i$ was detected by phosphorimager analysis (Applied Biosystems) and quantitated by volume quantitation using IMAGEQUANT (Molecular Dynamics).

Actin polymerization

Filament formation was monitored by observing the increase in fluorescence due to copolymerization of 2% pyrenyl-labelled bovine β/γ-actin [20] as described [12]. The dependence of elongation rate on actin concentration was determined as in [21]. The concentration of F-actin formed was calculated from the fluorescence signal by comparison with the values obtained with steady-state dilution of F-actin (2% pyrenyl-labelled) under identical conditions. The critical concentration for polymerization (A_{cc}) was estimated either from this experiment, or by using the sedimentation/DNase I inhibition assay [12]. High-shear viscometry was performed with sample volumes of 700 μL using Oswald–Manning viscometers with a buffer flow time of 56 s. When filament formation was induced with Mg^{2+}, the high-affinity divalent cation was exchanged to Mg^{2+} before the experiment, as described above.

Steady-state filament turnover

Monomeric actin was transferred by gel filtration (Sephadex G-25, Pharmacia) into G-buffer containing 0.1 mM εATP instead of 0.5 mM ATP. Samples (10 μM) in microtiter plates were induced to polymerize by addition of salt to 1 mM $MgCl_2$ and 100 mM KCl, and the reaction was allowed to reach steady state. Then, ATP (final conc. 0.5 mM) was added to each sample and the change in εATP fluorescence was recorded using a Fluoroscan II plate reader (Labsystems).

Fluorescence microscopy

Actin in G-buffer was polymerized (1 mM $MgCl_2$ and 100 mM KCl) in the presence of equimolar FITC-phalloidin. The polymerization reaction was allowed to proceed to steady state, before the samples were diluted to suitable concentrations, mounted in Vectashield (Vector Laboratories) and viewed in a Leica epifluorescence microscope.

Electron microscopy

Carbon-coated EM grids were incubated with actin samples, negatively stained with 1% uranyl acetate or 2% sodium silicotungstate and observed in a Hitachi H 7100 transmission electron microscope at 75 kV.

RESULTS

Isolation of mutant actins

Yeast-expressed wild-type and R177D-β-actins were purified using DNase I-affinity chromatography, and separated from the yeast actin by chromatography on hydroxyl apatite. The wild-type and mutant β-actins were displaced from the hydroxyl apatite column at similar salt concentrations implying that the surface properties of the mutant actin were not significantly altered by the amino acid replacement [22]. Also the successful isolation on DNase I-Sepharose suggested that the R177D mutation had not seriously distorted the conformation of the protein. This was confirmed by

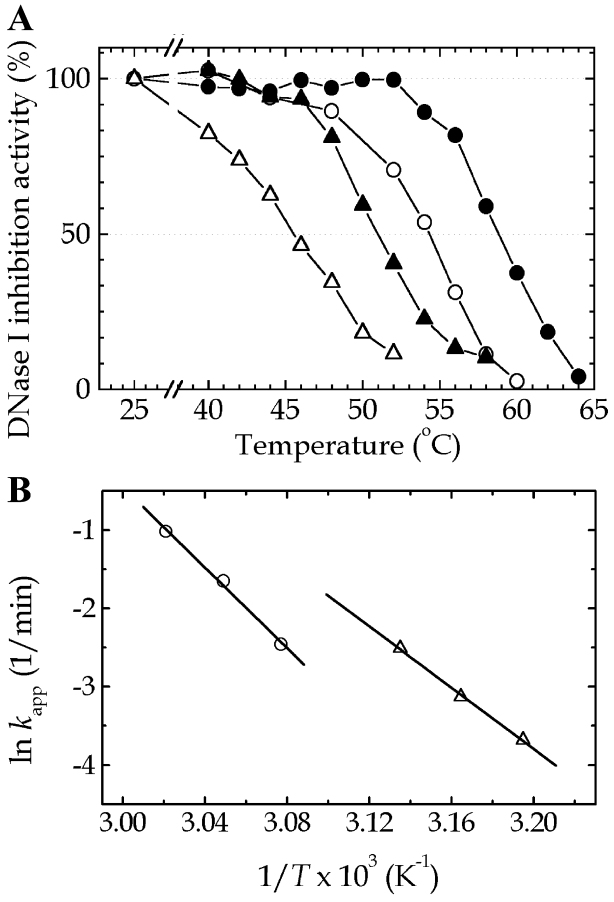

Fig. 2. Thermal stability of wild-type and R177D mutant actin. (A) Loss of DNase I inhibition activity during thermal unfolding. DNase I inhibition activites were measured while the actin samples were heated at a rate of 40 °C/h, and the remaining activities were plotted as percentage of the activities measured at 25 °C. Wild-type Ca-actin (●), wild-type Mg-actin (○), mutant Ca-actin (▲) and mutant Mg-actin (△). (B) Arrhenius plots of the apparent unfolding rate constants during incubation at constant temperatures. The activation energies for the unfolding reactions determined from these plots are 249 ± 30 kJ·mol^{-1} for wild-type Mg-actin (○) and 159 ± 6.4 kJ·mol^{-1} for R177D-Mg-actin (△).

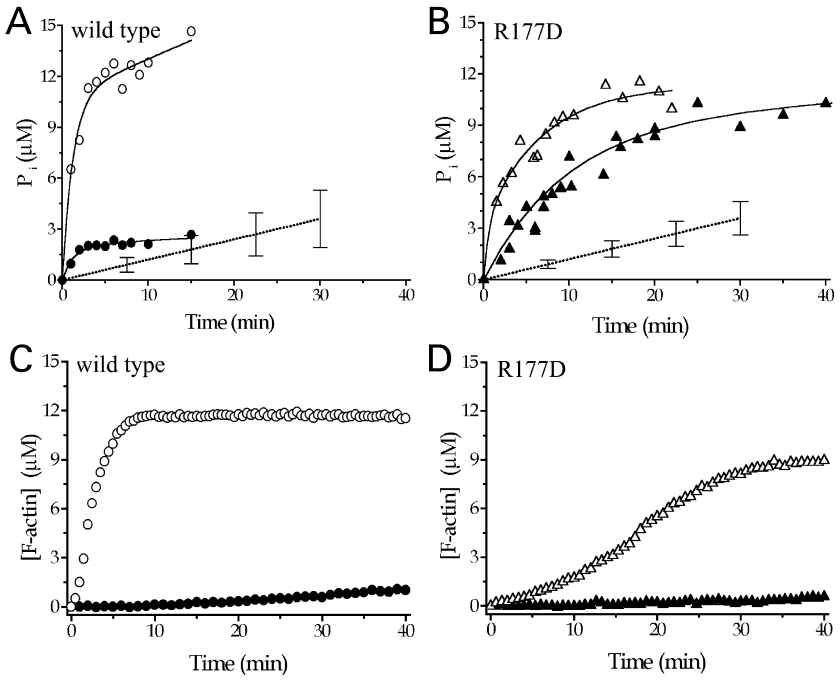

Fig. 3. ATPase activity during salt-induced polymerization of wild-type and R177D-actin. The generation of P_i (A,B) and the rise in pyrenyl fluorescence due to filament formation (C,D) were monitored after the addition of 1 mM $MgCl_2$ + 100 mM KCl to Mg-actins. (A,C) ATPase and polymerization of wild-type actin at concentrations of 2 μM (●) and 12 μM (○). (B,D) ATPase and polymerization of R177D-actin at concentrations of 3 μM (▲) and 12 μM (△). The dotted lines in (A) and (B) represent the ATPase activities of the actins at 12 μM when no salts were added (rate: 0.6 h^{-1}).

determination of the dissociation constants for the interaction of wild-type and mutant actin with DNase I. The K_d values obtained were 0.28 ± 0.04 nM for Ca-wild-type actin, 0.20 ± 0.04 nM for Ca-R177D-actin, 0.66 ± 0.09 nM for Mg/wild-type actin, and 0.62 ± 0.08 nM for Mg-R177D-actin. The K_d-value for the interaction between DNase I and Ca-actin is in agreement with that obtained with skeletal muscle α-actin [23], while the K_d for Mg-actin binding to DNase I has not been determined before.

Thermal stability of monomeric actin

The R177D-actin denatured at lower temperatures than wild-type actin (Fig. 2A). The melting temperatures were reduced from 59.0 °C to 52.0 °C for Ca-actin and from 54.0 to 45.0 °C for Mg-actin, and the decreased slope of the transition for mutant Mg-actin indicated a less cooperative unfolding. The activation energy for the thermal unfolding of Mg-actin was reduced from 249 ± 30 kJ·mol^{-1} to 159 ± 6.5 kJ·mol^{-1} by the mutation (Fig. 2B). The value determined for wild-type actin was similar to those reported for other actins [19].

Nucleotide exchange

As R177 is located in the vicinity of the nucleotide binding cleft (Fig. 1), it was important to see whether the mutation had changed the nucleotide binding properties of the protein. To do this, 6 μM ATP-actin in G-buffer, without excess ATP, were incubated with 300 μM of εATP and the increase in fluorescence due to εATP binding to actin was monitored. Under these conditions, rebinding of ATP is negligable, and the rate of incorporation of the fluorescent nucleotide therefore represents the off rate for ATP (k_{-ATP}) [24]. The mutation resulted in an increase in k_{-ATP} from $1.6 \pm 0.3 \times 10^{-2}$ s^{-1} to $2.4 \pm 0.2 \times 10^{-2}$ s^{-1} in Mg-actin, and from $2.9 \pm 0.2 \times 10^{-3}$ s^{-1} to $8.3 \pm 0.2 \times 10^{-3}$ s^{-1} in Ca-actin, suggesting that the mutant actin had a lower affinity for the nucleotide than the wild-type protein.

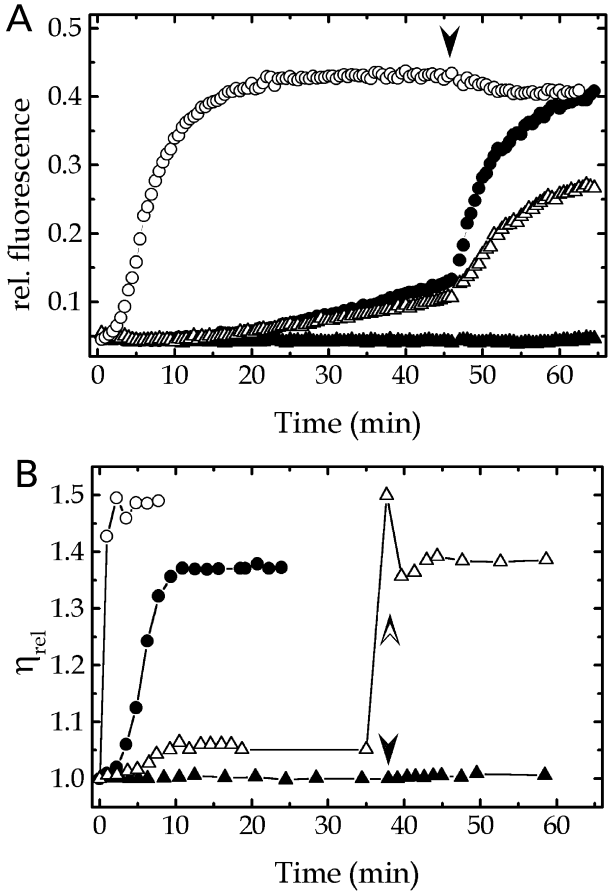

Fig. 4. Polymerization of wild-type and R177D-actin. (A) Pyrenyl fluorescence development after addition of 1 mM $MgCl_2$ + 100 mM KCl to 8 μM Ca- and Mg/wild-type actin (● and ○, respectively) or Ca- and Mg-R177D-actin (▲ and △, respectively). The arrow indicates addition of 1 mM $MgCl_2$ into the polymerization mixtures. (B) Viscosity analysis of Mg/wild-type (circles) and -mutant actins (triangles) polymerized by salt addition as in (A). The concentrations used were 8 μM (filled symbols) and 12 μM (open symbols). The solid and open arrows indicate addition of 1 mM $MgCl_2$ and 12 μM phalloidin, respectively, to R177D-actin.

Actin ATPase

Figure 3 shows the hydrolysis of ATP by wild-type and mutant actin (panels A and B, respectively) under nonpolymerizing (50 μm·mg^{-1}) and polymerizing conditions (Mg/K; 1 mM $MgCl_2$ plus 100 mM KCl) in correlation to filament formation as measured by the pyrenyl assay (panles C and D). The dotted lines in (A) and (B) illustrate the ATPase activity under low salt conditions (G-buffer). The results show that unpolymerized wild-type Mg-actin hydrolyzed ATP at a rate of 0.61 ± 0.29 h^{-1} ($n = 5$) at 25 °C, and that the R177D-actin had the same ATPase activity (0.60 ± 0.16·h^{-1}; $n = 6$). Thus, actin splits ATP without the involvement of an arginine at position 177.

The ATP hydrolysis observed under polymerizing conditions (Mg/K), with both wild-type and mutant Mg-actin (12 μM), clearly preceded filament formation. Comparison of Fig. 3A and C shows that ≈ 1 mol of ATP had been hydrolyzed per mol of actin at 2 min of reaction, whereas at this time point only about 30% of the actin had entered into polymeric form according to the pyrenyl assay. Similar results were obtained earlier with wild-type and different mutant β-actins [12]. As the polymerization reaction reached steady state, the ATP hydrolysis entered a second phase of much lower rate thought to reflect monomer association/dissociation at filament ends (treadmilling). At 2 μM Mg-actin, the ATPase activity almost ceased when one molecule of ATP had been hydrolyzed per actin monomer (Fig. 3A). Here, polymer formation was slow and clearly hydrolysis of ATP ceased long before polymers were detected. This suggests that ATP hydrolysis takes place already during nucleation.

Mutant actin hydrolyzed ATP rather rapidly even at an actin concentration of 3 μM (Fig. 3B, filled triangles), which is close to the critical concentration of polymerization (Table 1). After an initial phase, the reaction rate began to decline, and had levelled off after 10–15 min, when about 3 mol of ATP had been hydrolyzed per mole of actin (Fig. 3B). Even at this stage, there was no detectable filament formation (Fig. 3D), and the actin inhibited DNase I with an activity characteristic of the unpolymerized protein (not shown). The decrease in ATPase activity therefore did not appear to be due to inactivation of the protein. At actin concentrations well above A_{cc} (12 μM), ATP was hydrolyzed in equimolar amounts to actin, after which the hydrolysis decreased (Fig. 3B, open triangles). Also here ATP was hydrolyzed in advance of polymer formation.

Actin polymerization

As shown in Fig. 4A, addition of polymerizing salts (Mg/K) to wild-type Mg-actin at 8 μM, after a short lag phase, resulted in a rapid increase in pyrenyl fluorescence, indicating actin filament formation (open circles). The reaction reached steady state after about 15 min, and addition of extra $MgCl_2$ did not change the steady state level of polymerization. Attempts to induce polymerization of Ca-actin by the addition of KCl to 100 mM (no Mg^{2+}) caused only a slow increase in pyrenyl fluorescence over a period of 45 min. If $MgCl_2$ (1 mM) was added at this stage, there was a rapid increase in fluorescence (filled circles), which reached the same steady state level as with Mg-actin induced to polymerize by the addition of $MgCl_2$ as described above.

The mutant Ca-actin (8 μM), on the other hand, did not appear to form polymers in 100 mM KCl, and addition of 1 mM $MgCl_2$ had no effect on the fluorescence of the added pyrenyl actin during the time period studied. When Mg/K was added to mutant Mg-actin, there was a slow increase in fluorescence (open triangles) and addition of extra $MgCl_2$ accelerated this increase. The steady state level of fluorescence reached by the mutant actin was about 60% of that seen with wild-type actin.

Monitoring polymerization of the wild-type Mg-actin (8 and 12 μM; Mg/K-milieu) using high-shear viscometry showed a rise in viscosity (Fig. 4B), which occurred on a time scale similar to that seen with the pyrenyl assay (compare Fig. 3C; 12 μM). However, mutant Mg-actin at 8 μM (closed triangles), showed no increase in viscosity under the same conditions, not even after addition of extra Mg^{2+} (to 2 mM). Here, the pyrenyl signal (Fig. 4A, open triangles) approached two-thirds of that of the wild-type indicating that polymers had formed, which were not registered by viscometry. At 12 μM, the mutant actin in the Mg/K-milieu gave rise to a small increase in viscosity, which finally reached a level which was about one tenth of that observed with wild-type actin under the same conditions (open triangles). However, if phalloidin was added at this stage, there was an immediate increase in the viscosity. Together with the results shown in Fig. 3C,D, these observations suggest that Mg-R177D-actin formed short and/or fragile filaments that were converted into long, stable filaments upon phalloidin-binding. Fluorescence and electron microscopy confirmed the presence of long filaments of R177D-actin in the presence of phalloidin, as discussed below.

Table 1. Steady-state concentrations of unpolymerized wild-type and R177D-actin (A_{cc}) under different salt conditions. The values for A_{cc} are given in μM and were determined by either steady-state dilution of pyrenyl-labeled actin (a) or by the sedimentation/DNase I-binding assay (b). Salt conditions indicate the divalent cation (Mg^{2+}/Ca^{2+}) present in the high-affinity site in G-actin before salt addition, and the final conditions used to induce polymerization. Rh-phalloidin, rhodamine phalloidin. ND, not determined.

	Wild-type		R177D	
Salt conditions	a	b	a	b
Mg^{2+}/1 mM Mg^{2+} + 0.1 M K^+	0.47	0.48	3.2	5.8
Mg^{2+}/2 mM Mg^{2+} + 0.1 M K^+	ND	0.28	ND	4.5
Mg^{2+}/1 mM Mg^{2+} + 0.1 M K^+ + 5 μM phalloidin	0.18	0.16	1.5	1.6
Mg^{2+}/1 mM Mg^{2+} + 0.1 M K^+ + 5 μM Rh-phalloidin	0.18	ND	1.5	ND
Mg^{2+}/0.1 M K^+	1.45	1.46	4.6	> 12.0
Ca^{2+}/0.1 M K^+	4.0	4.1	> 12.0	> 12.0

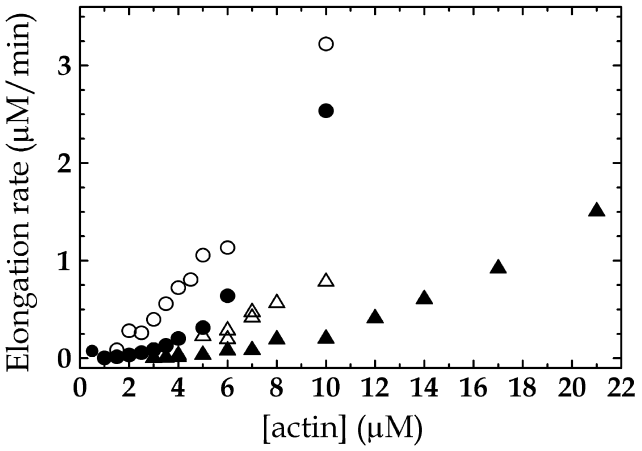

Fig. 5. Filament elongation rates as a function of actin concentration. Wild-type (circles) and R177D-mutant actins (triangles) were co-polymerized with 2% pyrenyl-actin in 1 mM $MgCl_2$ and 100 mM KCl. Experiments were conducted unseeded (filled symbols) or with addition of 1 μM unlabelled F-actin seed solution together with the polymerizing salts (open symbols).

The R177D mutation resulted in an approximately 10-fold increase in the critical concentration for polymerization, A_{cc}, under the salt conditions studied (Table 1). For R177D-actin, the A_{cc} values measured with the sedimentation/DNase I inhibition assay were higher than those measured using pyrenyl fluorescence, except when phalloidin was present. This difference could be due to failure of short oligomers to sediment, or to filament fragmentation or partial depolymerization caused by the exposure of the filaments to high gravitational forces during ultracentrifugation. Phalloidin decreased the A_{cc} twofold to threefold for both mutant and wild-type actin (Table 1), and rhodamine-phalloidin had a similar effect.

The dependence of the elongation rates on actin concentration was studied in the Mg/K-milieu in the presence and absence of 1 μM wild-type F-actin seeds using the pyrenyl assay. The results are presented as a plot of the elongation rates vs. actin concentration using the equation:

$$-\frac{dc}{dt} = k_+c - k_-$$

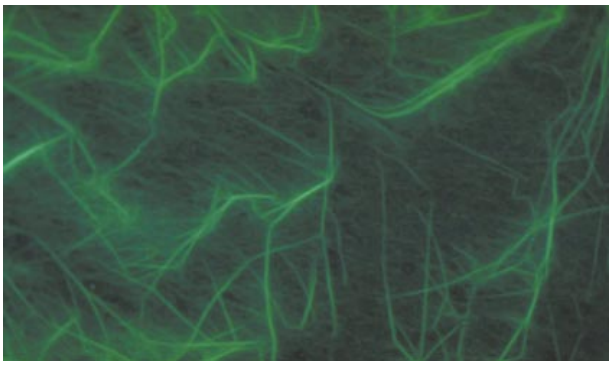

Fig. 6. Fluorescence micrograph of R177D-β-actin filaments stained with FITC-phalloidin. F-actin in the presence of equimolar FITC-phalloidin was diluted to a suitable concentration and observed by epifluorescence microscopy.

where c is the monomer concentration, and k_+ and k_- the monomer association and dissociation rate constants, respectively, as described by Oosawa & Asakura [25]. As shown in Fig. 5, the analysis of both wild-type and mutant β-actin, seeded or nonseeded, gave rise to curves of the same general appearance [26], i.e. with low slopes in the lower concentration range and a pronounced increase in slope at higher concentrations. At about 5 μM with wild-type β-actin and 10 μM with the R177D mutant actin (both nonseeded), the slope of the curves increased significantly. With the mutant actin, the slopes were much lower than with the wild-type, demonstrating the poor polymerizability of the mutant. In the presence of F-actin seeds (1 μM), the slope of the concentration-dependent increase in elongation rate was constant over the whole concentration range for both actins. Seeding increased the elongation rates for R177D-actin, but not to wild-type levels.

Filament morphology

Fluorescence microscopy of mutant actin filament solutions incubated with FITC-phalloidin revealed labeled filaments (Fig. 6), directly demonstrating that phalloidin interacts with filaments consisting of R177D-actin. Electron microscopy of wild-type and R177D-actin filaments, without and with phalloidin, did not reveal any differences in structure. However, in the case of the mutant actin, the filament density on the grids was lower, and a background of amorphous material was seen. Samples of mutant actin withdrawn from the viscometer contained less filaments compared to nonsheared samples of the same actin.

DISCUSSION

Amongst the actin-fold family of proteins, the mechanism of ATP hydrolysis is best understood for the 44-kDa ATPase fragment of Hsc70. On the basis of crystal structures of the protein, it was proposed that K71 in Hsc70 participates in hydrolysis of ATP by stabilizing a water molecule, or a hydroxyl ion, for nucleophilic attack on the γ-phosphate [27]. This model was supported by mutagenesis of K71, which abolished the ATPase activity [6]. The close structural relationship of Hsc70 and actin, and the analogous positioning of arginine 177 of actin with lysine 71 of Hsc70 suggested that the two proteins might utilize a similar mechanism for ATP hydrolysis. This is apparently supported by the abolition of the ATPase activity of actin by ADP-ribosylation of R177 by bacterial toxins [9]. However, the results presented here demonstrate that R177 is not directly involved in the hydrolysis of ATP by actin. This in turn suggests that the covalent modification of R177 by bacterial toxins inhibits the ATPase activity not by elimination of a catalytically important residue [8,9], but rather by displacing other residues involved in the catalysis, or by interfering with the coordinated motions of these residues during polymerization.

Arginine 177 is important for actin stability

In the DNase I:actin and the tight-state profilin:actin crystals [2,4], the guanidinium group of R177 forms a salt cluster across the interdomain cleft involving the carboxyl group of D179 and the carbonyl oxygen of H73. Thus, the R177 can be perceived as a 'clamp' over the nucleotide-binding cleft (Fig. 1), and it is expected that loosening of the interdomain bonding network would destabilize the molecule, as discussed for other actin mutants [12,28]. The decrease in thermostability and the

increase in the nucleotide exchange rate seen with the mutant protein confirm that R177 is a key residue controling relative interdomain motions.

Binding of R177D-actin to DNase I

It was shown earlier that exchange of high-affinity Ca^{2+} for Mg^{2+} on wild-type actin causes a weakened interdomain coupling [19]. This change was accompanied by a threefold decrease in affinity for DNase I (see earlier). The K_d for the interaction of R177D-actin with DNase I was unchanged compared to the wild-type values, regardless of whether it was in the Ca- or Mg-form. Thus, despite a disturbed interdomain relationship in the mutant actin, it bound DNase I with different affinities depending on the divalent cation bound. This suggests that the relative positioning of subdomains 2 and 4, both of which comprise the DNase I-binding site on actin, was preserved well enough to allow binding of DNase I with unchanged affinity.

Polymerization and ATPase activity of wild-type and mutant actin

In the presence of Mg^{2+}-ions, the dissociation constant for the (+)-end of the filament is about 0.1 μM and that of the (−)-end 0.7 μM (reviewed in [29]). Thus, between 0.1 and 0.7 μM growth of actin filaments takes place at the (+)-end. The rate of growth increases with increasing concentration of actin monomers in this concentration interval, but is accompanied by slow depolymerization at the (−)-end of the filaments. At concentrations above the A_{cc} for the (−)-end, i.e. 0.7 μM, growth at the (−)-end adds to the total growth of the filaments. Increasing the actin concentrations even further would lead to accelerated nucleation increasing the number of growing filaments, resulting in a nonlinear increase in the elongation rate. This scenario explains the general behavior of both wild-type and mutant actin in experiments where the dependence of elongation rate on actin concentration is compared (Fig. 5).

With wild-type Mg-actin, ATP hydrolysis preceded polymer formation, and after the actin had hydrolyzed approximately stoichiometric amounts of ATP, the hydrolysis rate decreased significantly, as expected by the greatly reduced rate of ATP exchange in actin monomers incorporated into filaments. The slow, continued hydrolysis reflects association/dissociation of actin monomers at filament ends. The results presented in Figs 3D, 4 and 5 suggest that nucleation as well as elongation of actin filaments are impaired in the case of the mutant actin. The experiments correlating mutant actin polymerization with ATP hydrolysis (Fig. 3) revealed an unexpected complexity. As for the wild-type, the mutant actin at concentrations well above A_{cc} hydrolyzed a stoichiometric amount of ATP. However, in the polymerization experiment carried out at 3 μM R177D actin, more than stoichiometric amounts of ATP were hydrolyzed, reaching a level corresponding to three molecules per actin monomer. Furthermore, hydrolysis of the nucleotide by the mutant actin preceded polymer formation to a greater extent than for wild-type actin (compare Fig. 3B and D). Regardless of the actin isoform, filament formation generally takes place ahead of ATP hydrolysis under conditions of fast elongation. Under conditions which result in slower filament elongation, e.g. in the absence of F-actin seeds [30,31] or at lower total actin concentration [31,32], the lag phase for ATP hydrolysis decreases significantly relative to filament formation. The fast ATP hydrolysis by β-actin and in particular by the mutant actin represent an extreme case of what has already been reported for muscle actin, as these two actins nucleate more slowly than muscle actin. Thus apparently in the mutant actin nuclei or oligomeric actin structures were formed but quickly dissociated, allowing cycles of ATP hydrolysis to take place, as observed in other systems [33]. Therefore, salt addition stimulates both filament formation and the ATPase activity. However, unlike polymerization, the actin ATPase does not have a critical concentration. The subsequent levelling off of the ATP hydrolysis (sub-A_{cc}) implies that the actin eventually was transformed into a state where nucleotide exchange was limited, perhaps related to a state resembling that found in F-actin. Denaturation was ruled out as an explanation for this levelling off, because actin taken at the end of the experiment in Fig. 3 retained full activity in inhibiting DNase I. Thus, the decline in the rate of ATP hydrolysis showed that filamentous structures had formed, even though the product did not give any pyrenyl signal. This indicates that the final incorporation of the actin, especially with respect to the final conformation of the C-terminus where the pyrenyl is located, failed to follow the wild-type pattern [34,35].

Phalloidin-binding and filament morphology

Phalloidin binds to filamentous actin, in a 1 : 1 stoichiometry with respect to actin monomers, and lowers the A_{cc} [36,37], resulting in an apparent stabilization of the filaments. It is shown here that the R177D mutation caused a large increase in A_{cc}, and that phalloidin binding decreased A_{cc} twofold to threefold, although not to the low levels reached with wild-type actin. This effect of phalloidin, and the binding of FITC-phalloidin (and rhodamine-phalloidin) to the filaments polymerized from the R177D-actin shows that R177 itself is not required for phalloidin-binding. Belmont *et al.* [10] analyzed an R177A mutant with respect to the *in vitro* binding of phalloidin to actin filaments and found no binding. These conflicting results could depend on the different experimental conditions.

Mutagenesis of the endogenous actin gene in yeast has shown that replacing R177, D179, or G158 with alanine prevents phalloidin staining of actin structures in mutated cells [10], suggesting that these residues are part of a phalloidin binding site. Vandekerckhove *et al.* [38] used two types of affinity-labelling derivatives of phalloidin. One established a covalent link with E117, and the other reacted with M119 and M355. The E117 and M119 are on the same side of the actin monomer as R177, D179 and G158, whereas M355 is on the opposite side. However, in both cases the cross-linker was too long to pinpoint the phalloidin binding site. Lorenz *et al.* [39], using a 'directed mutation algorithm', placed the phalloidin site at the intersection of three actin subunits in the Holmes–Lorenz model of F-actin, close to the fiber axis. However, there are doubts about this analysis. For example, the number of refined parameters in the model greatly exceeds the number of experimental observations [40], and the refinement process did not include diffraction data from both free and phalloidin-bound actin filaments. Instead, diffraction patterns calculated with the atomic model having phalloidin positioned at various sites were compared with experimental X-ray diffraction patterns obtained from oriented gels of F-actin containing phalloidin. The position arrived at for phalloidin was the one giving the lowest R-factor, rather than one determined on the basis of difference Fourier maps. Thus, as the actual electron density for phalloidin was not obtained by Lorenz *et al.* [39] its positioning relative to the filament axis must be regarded as tentative.

Finally, cryo-electron microscopy of actin filaments labelled with clusters of undecagold bound to phalloidin via a 2-nm linker, imaged the gold particles at a radius of 3 nm from the filament axis [41]. Steinmetz *et al*. [41] have shown that this position is compatible with phalloidin cross-linking data [38] and the results obtained with mutagenesis of yeast actin [11], assuming the monomer orientation in the Holmes–Lorenz model of F-actin. It was also concluded that an F-actin model based on the actin ribbon seen in the profilin:β-actin crystal could not account for the position of the gold particles. However, in modelling the position of gold-labelled phalloidin on the side of the monomer in the ribbon-derived filament opposite that expected from mutagenesis data [41], it was assumed that the position of phalloidin relative to the fiber axis had been determined unambiguosly by Lorenz *et al*. [39] (see earlier). If instead the gold-labelled phalloidin had been placed over the phosphate-binding loops near G158, R177 and D179, in conformance with the mutagenesis data on yeast actin [10], both the cross-linking results and the position of the gold label could be accounted for with models resulting from the ribbon-to-helix conjecture, including the one presented [41]. Therefore, caution should be exercised in interpreting mutagenesis data solely in terms of one specific atomic model.

Concluding remarks

The extensive characterization of β-actin points to a crucial difference between α- and β-actin with respect to the polymerization behaviour. This might be related to the recent finding that skeletal muscle α-actin prepared from acetone powder contains nucleating factors [42]. The present work shows that R177 plays an essential role in formation of the final filamentous structure assembled from β-actin-ADP·P_i-monomers. It has been discovered recently that yeast-expressed β-actin is not post-translationally methylated at histidine 73 [43]. Even though the expected effects of this modification on the polymerization behaviour of chicken β-actin are subtle, wild-type chicken β-actin expressed in yeast was used in the control experiments in this work.

By virtue of spanning the nucleotide-binding cleft, the R177 side chain may be sensitive to conformational changes accompanying the release of P_i. It is of interest to note that phalloidin increases the intrinsic rate of ATP-hydrolysis, but strongly inhibits P_i-release [44,45]. Thus, the return to the F-actin.ADP ground state upon P_i-release can be coupled to a change in the actin monomer that may be mediated by R177, and this process could be critical in the formation of the native actin filament. This accords well with observations made with yeast actin upon mutating valine 159, located in the vicinity of R177, to an asparagine, where changes in structure and stability of actin filaments occur [46,47]. The filaments formed by V159N actin resemble BeF_x-treated ADP-actin filaments, as observed by cryo-electron microscopy [47], again pointing to the region around these residues as important in governing release of inorganic phosphate from polymerizing actin. The emerging view of actin polymerization is that ATP-containing actin monomers add primarily to the (+)-end of filaments, hydrolyze ATP, and undergo a conformational change to a state of lower Gibbs free energy associated with release of phosphate. R177 appears to play a critical role in coordinating these conformational changes. The nature of this conformational change, however, can only be elucidated by determination of the structure of the actin filament.

ACKNOWLEDGEMENTS

We acknowledge financial support from the Swedish National Science Research Council (NFR) to U. L. and R. K., from the Swedish Foundation for International Cooperation in Research and Higher Education (STINT) to U. L., and from the NIH (GM44038) to C. E. S.

REFERENCES

1. Bork, P., Sander, C. & Valencia, A. (1992) An ATPase domain common to prokaryotic cell cycle proteins, sugar kinases, actin, and hsp70 heat shock proteins. *Proc. Natl Acad. Sci. USA* **89**, 7290–7294.
2. Kabsch, W., Mannherz, H.G., Suck, D., Pai, E.F. & Holmes, K.C. (1990) Atomic structure of the actin:DNase I complex. *Nature* **347**, 37–44.
3. McLaughlin, P.J., Gooch, J.T., Mannherz, H.G. & Weeds, A.G. (1993) Structure of gelsolin segment 1-actin complex and the mechanism of filament severing. *Nature* **364**, 685–692.
4. Schutt, C.E., Myslik, J.C., Rozycki, M.D., Goonesekere, N.C. & Lindberg, U. (1993) The structure of crystalline profilin-beta-actin. *Nature* **365**, 810–816.
5. Chik, J.K., Lindberg, U. & Schutt, C.E. (1996) The structure of an open state of beta-actin at 2.65 Å resolution. *J. Mol. Biol.* **263**, 607–623.
6. O'Brien, M.C., Flaherty, K.M. & McKay, D.B. (1996) Lysine 71 of the chaperone protein Hsc70 Is essential for ATP hydrolysis. *J. Biol. Chem.* **271**, 15874–15878.
7. Aktories, K. & Wegner, A. (1989) ADP-ribosylation of actin by clostridial toxins. *J. Cell Biol.* **109**, 1385–1387.
8. Geipel, U., Just, I., Schering, B., Haas, D. & Aktories, K. (1989) ADP-ribosylation of actin causes increase in the rate of ATP exchange and inhibition of ATP hydrolysis. *Eur. J. Biochem.* **179**, 229–232.
9. Sehr, P., Just, I. & Aktories, K. (1996) ADP-ribosylation of actin by Clostridium perfringens iota toxin and turkey erythrocyte ADP-ribosyltransferase A: effects on profilin-regulated nucleotide exchange and ATPase activity. *Naunyn Schmiedebergs Arch. Pharmacol.* **354**, 693–697.
10. Belmont, L.D., Patterson, G.M. & Drubin, D.G. (1999) New actin mutants allow further characterization of the nucleotide binding cleft and drug binding sites. *J. Cell Sci.* **112**, 1325–1336.
11. Wertman, K.F., Drubin, D.G. & Botstein, D. (1992) Systematic mutational analysis of the yeast ACTI gene. *Genetics* **132**, 337–350.
12. Schüler, H., Korenbaum, E., Schutt, C.E., Lindberg, U. & Karlsson, R. (1999) Mutational analysis of Ser14 and Asp157 in the nucleotide-binding site of beta-actin. *Eur. J. Biochem.* **265**, 210–220.
13. Karlsson, R. (1988) Expression of chicken beta-actin in *Saccharomyces cerevisiae*. *Gene* **68**, 249–257.
14. Houk, T.W. Jr & Ue, K. (1974) The measurement of actin concentration in solution: a comparison of methods. *Anal. Biochem.* **62**, 66–74.
15. Gershman, L.C., Newman, J., Selden, L.A. & Estes, J.E. (1984) Bound-cation exchange affects the lag phase in actin polymerization. *Biochemistry* **23**, 2199–2203.
16. Lindberg, U., Schutt, C.E., Hellsten, E., Tjader, A.C. & Hult, T. (1988) The use of poly (L-proline)-Sepharose in the isolation of profilin and profilactin complexes. *Biochim. Biophys. Acta* **967**, 391–400.
17. Blikstad, I., Markey, F., Carlsson, L., Persson, T. & Lindberg, U. (1978) Selective assay of monomeric and filamentous actin in cell extracts, using inhibition of deoxyribonuclease I. *Cell* **15**, 935–943.
18. Secrist, J.A.D., Barrio, J.R., Leonard, N.J., Villar-Palasi, C. & Gilman, A.G. (1972) Fluorescent modification of adenosine 3′,5′-monophosphate: spectroscopic properties and activity in enzyme systems. *Science* **177**, 279–280.
19. Schüler, H., Lindberg, U., Schutt, C.E. & Karlsson, R. (2000) Thermal unfolding of G-actin monitored with the DNase I-inhibition assay Stabilities of actin isoforms. *Eur. J. Biochem.* **267**, 476–486.
20. Kouyama, T. & Mihashi, K. (1981) Fluorimetry study of *N*-(1-pyrenyl) iodoacetamide-labelled F-actin. Local structural change of actin protomer both on polymerization and on binding of heavy meromyosin. *Eur. J. Biochem.* **114**, 33–38.
21. Selden, L.A., Gershman, L.C. & Estes, J.E. (1986) A kinetic

comparison between Mg-actin and Ca-actin. *J. Muscle. Res. Cell Motil.* **7**, 215–224.
22. Gorbunoff, M.J. & Timasheff, S.N. (1984) The interaction of proteins with hydroxyapatite. III. Mechanism. *Anal. Biochem.* **136**, 440–445.
23. Mannherz, H.G., Goody, R.S., Konrad, M. & Nowak, E. (1980) The interaction of bovine pancreatic deoxyribonuclease I and skeletal muscle actin. *Eur. J. Biochem.* **104**, 367–379.
24. Kinosian, H.J., Selden, L.A., Estes, J.E. & Gershman, L.C. (1993) Nucleotide binding to actin. Cation dependence of nucleotide dissociation and exchange rates. *J. Biol. Chem.* **268**, 8683–8691.
25. Oosawa, F. & Asakura, S. (1975) *Thermodynamics of the Polymerization of Protein.* Academic Press, New York, USA.
26. Carlier, M.F. (1989) Role of nucleotide hydrolysis in the dynamics of actin filaments and microtubules. *Int. Rev. Cytol.* **115**, 139–170.
27. Flaherty, K.M., Wilbanks, S.M., DeLuca-Flaherty, C. & McKay, D.B. (1994) Structural basis of the 70-kilodalton heat shock cognate protein ATP hydrolytic activity. II. Structure of the active site with ADP or ATP bound to wild type and mutant ATPase fragment. *J. Biol. Chem.* **269**, 12899–12907.
28. Chen, X., Peng, J., Pedram, M., Swenson, C.A. & Rubenstein, P.A. (1995) The effect of the S14A mutation on the conformation and thermostability of *Saccharomyces cerevisiae* G-actin and its interaction with adenine nucleotides. *J. Biol. Chem.* **270**, 11415–11423.
29. Sheterline, P., Clayton, J. & Sparrow, J. (1998) Actin. *Protein Profile* **4**, 1–119.
30. Pollard, T.D. & Weeds, A.G. (1984) The rate constant for ATP hydrolysis by polymerized actin. *FEBS Lett.* **170**, 94–98.
31. Ohm, T. & Wegner, A. (1994) Mechanism of ATP hydrolysis by polymeric actin. *Biochim. Biophys. Acta* **1208**, 8–14.
32. Carlier, M.F., Pantaloni, D. & Korn, E.D. (1987) The mechanisms of ATP hydrolysis accompanying the polymerization of Mg-actin and Ca-actin. *J. Biol. Chem.* **262**, 3052–3059.
33. Fievez, S., Pantaloni, D. & Carlier, M.F. (1997) Kinetics of myosin subfragment-1-induced condensation of G-actin into oligomers, precursors in the assembly of F-actin-S1. Role of the tightly bound metal ion and ATP hydrolysis. *Biochemistry* **36**, 11837–11842.
34. Aspenström, P., Schutt, C.E., Lindberg, U. & Karlsson, R. (1993) Mutations in beta-actin: influence on polymer formation and on interactions with myosin and profilin. *FEBS Lett.* **329**, 163–170.
35. Strzelecka-Golaszewska, H., Mossakowska, M., Wozniak, A., Moraczewska, J. & Nakayama, H. (1995) Long-range conformational effects of proteolytic removal of the last three residues of actin. *Biochem. J.* **307**, 527–534.
36. Lengsfeld, A.M., Low, I., Wieland, T., Dancker, P. & Hasselbach, W. (1974) Interaction of phalloidin with actin. *Proc. Natl Acad. Sci. USA* **71**, 2803–2807.
37. Wieland, T. & Faulstich, H. (1978) Amatoxins, phallotoxins, phallolysin, and antamanide: the biologically active components of poisonous *Amanita* mushrooms. *CRC Crit. Rev. Biochem.* **5**, 185–260.
38. Vandekerckhove, J., Deboben, A., Nassal, M. & Wieland, T. (1985) The phalloidin binding site of F-actin. *EMBO J.* **4**, 2815–2818.
39. Lorenz, M., Popp, D. & Holmes, K.C. (1993) Refinement of the F-actin model against X-ray fiber diffraction data by the use of a directed mutation algorithm. *J. Mol. Biol.* **234**, 826–836.
40. Schutt, C.E., Rozycki, M.D., Myslik, J.C. & Lindberg, U. (1995) A discourse on modeling F-actin. *J. Struct. Biol.* **115**, 186–198.
41. Steinmetz, M.O., Stoffler, D., Muller, S.A., Jahn, W., Wolpensinger, B., Goldie, K.N., Engel, A., Faulstich, H. & Aebi, U. (1998) Evaluating atomic models of F-actin with an undecagold-tagged phalloidin derivative. *J. Mol. Biol.* **276**, 1–6.
42. Selden, L.A., Kinosian, H.J., Estes, J.E. & Gershman, L.C. (2000) Cross-linked dimers with nucleating activity in actin prepared from muscle acetone powder. *Biochemistry* **39**, 64–74.
43. Kalhor, H.R., Niewmierzycka, A., Faull, K.F., Yao, X., Grade, S., Clarke, S. & Rubenstein, P.A. (1999) A highly conserved 3-methylhistidine modification is absent in yeast actin. *Arch. Biochem. Biophys.* **370**, 105–111.
44. Pinaev, G., Schutt, C.E. & Lindberg, U. (1995) The effect on actin ATPase of phalloidin and tetramethylrhodamine phalloidin. *FEBS Lett.* **369**, 144–148.
45. Dancker, P. & Hess, L. (1990) Phalloidin reduces the release of inorganic phosphate during actin polymerization. *Biochim. Biophys. Acta* **1035**, 197–200.
46. Belmont, L.D. & Drubin, D.G. (1998) The yeast V159N actin mutant reveals roles for actin dynamics *in vivo*. *J. Cell Biol.* **142**, 1289–1299.
47. Belmont, L.D., Orlova, A., Drubin, D.G. & Egelman, E.H. (1999) A change in actin conformation associated with filament instability after P_i release. *Proc. Natl Acad. Sci. USA* **96**, 29–34.
48. Kraulis, P.J. (1991) MOLSCRIPT: a program to produce both detailed and schematic plots of protein structures. *J. Appl. Crystallogr.* **24**, 946–950.